Suominen, Mikko; Kujala, Pentti; Romanoff, Jani; Remes, Heikki

The effect of the extension of the instrumentation on the measured ice-induced load on a ship hull

Published in:
Ocean Engineering

DOI:
10.1016/j.oceaneng.2017.09.056

Published: 01/01/2017

Document Version
Publisher's PDF, also known as Version of record

Ocean Engineering 144 (2017) 327–339

Contents lists available at ScienceDirect

Ocean Engineering

journal homepage: www.elsevier.com/locate/oceaneng

The effect of the extension of the instrumentation on the measured ice-induced load on a ship hull

Mikko Suominen *, Pentti Kujala, Jani Romanoff, Heikki Remes

Aalto University, School of Engineering, Department of Mechanical Engineering, PO Box 15300, FI-00076, Aalto, Finland

ARTICLE INFO

Keywords:
Ice load
Full-scale
Uncertainty in measurements
Load length
The extension of the instrumentation

ABSTRACT

Due to the complexity of the ice-structure interaction, the knowledge about the ice-induced loads on a ship hull has been gained from full-scale measurements. As the instrumentation of the hull for the measurements is expensive, the extension is concerned at the planning phase. However, a narrow instrumentation can cause an error in the measurements, as the response of the adjacent frames with respect to the observed frame is not known. Thus, this paper studies the differences between loads measured from one or several frames on board S.A. Agulhas II. The difference results from the ability of the structure to transport loading internally. The results show that when the loads affect only an individual frame, the instrumentations give similar results. However, the difference increases with the load length and the loading that is determined can be 15% higher for one frame instrumentation for a structure similar to the aft shoulder of S.A. Agulhas II. Furthermore, the difference in the mean value and standard deviation of the measurement time histories can be up to 10%. The study presents a new efficient method to obtain a rough estimate of the possible difference in the measured results between extensive and narrow instrumentation.

1. Introduction

Maritime transportation offers an efficient way to transport large quantities of goods and raw material. As some of the routes lie at higher latitudes, e.g. in the Great Lakes, the Baltic Sea, and the Arctic, the ships operating in these areas have to be capable of operating in ice conditions. In order to secure their safety, the structure of the ships has to be designed for these conditions. From the structural design point of view, the magnitude and extent of the external loading are of interest. Ice-induced loading and structural response under the loading have been studied numerically (see e.g. Su et al., 2011), with laboratory experiments (see e.g. Kim and Quinton, 2016) and full-scale measurements (see e.g. Ehlers et al., 2015). However, the ice-breaking process is fairly complex due to the variation in the ice conditions (e.g. strength, thickness, first- or multi-year ice), ship operations (e.g. manoeuvres), and in the location and area of the contact (e.g. ship shoulder, mid-ship). The benefit of full-scale measurements in comparison to the numerical methods and experiments is that all the variations are embedded in the measurements. Therefore, knowledge obtained from full-scale measurements has crucial importance.

Different techniques to measure full-scale ice loads on a ship hull have been utilized. As the ice pressure on a small area can be significant – see e.g. Sanderson (1988) and Taylor et al. (2010) – external foils do not last long outside the hull; see e.g. the measurements by Riska et al. (1990) with a polyvinylidene difluoride (PVDF) film. Alternative ways of measuring the pressure pattern outside the hull have been developed that employ additional construction that can survive the ice contact (Gagnon, 2008). However, these types of solutions can alter the stiffness of the structure, which affects the load-carrying mechanism of the hull structure and possibly also the load magnitude. Thus, the ice-induced loading is commonly measured by measuring the shear strain difference at the ends of the transverse frames, as it is assumed that the load transfer is mainly due to shear along this frame (see e.g. Riska et al., 1983; Kujala and Vuorio, 1986; St. John et al., 1994; Ritch et al., 2008; Suominen et al., 2013). In these type of measurements, the loading is determined from the strain-force relation.

Although all the variations are embedded in the full-scale measurements, the measurements contain uncertainty related to the determination of the force from the measured strain. The uncertainty arises from the assumptions on the loading conditions in the determination of the strain-force relation and from the extension of the instrumentation. The ice-frames are connected to the adjacent frames via typically relatively thick hull plating. As the plates are thick, the plates also transfer the loads imposed on a single frame directly to adjacent frames, but also

* Corresponding author.
E-mail address: mikko.suominen@aalto.fi (M. Suominen).

https://doi.org/10.1016/j.oceaneng.2017.09.056
Received 21 March 2017; Received in revised form 22 August 2017; Accepted 24 September 2017
Available online 7 October 2017

to the supporting web-frames directly. If adjacent frames are instrumented, an influence coefficient matrix can be applied in order to account for the effect of the adjacent frames on the measurements (see e.g. Riska et al., 1983; Ship Structure Committee, 1990; Ralph et al., 2003; Suominen et al., 2017). Commonly, the influence matrix is defined by employing finite element analysis (FEA). The extent of the instrumentation in a specific area has varied from a single frame – see e.g. Kujala, 1989 – to several adjacent frames (see e.g. St. John et al., 1994; Ritch et al., 2008; Suominen et al., 2013). In a case single frame is instrumented, the influence coefficient matrix cannot be applied and uncertainty is increased.

Although the internal load distribution between the frames has been studied, the knowledge has not been applied to the thorough estimation of the uncertainty of the full-scale measurements. Earlier studies have estimated the effect of the calibration load length – see e.g. Kujala (1989) – and the effect of accounting for the adjacent frames when the loading on a frame is observed (Kujala and Vuorio, 1986; Ship Structure Committee, 1990). Although these studies provided rough estimates of the uncertainty, the uncertainty analysis has not been applied extensively to full-scale measurements. When only one frame is instrumented, the possible overestimation or underestimation of the external loading depends on the ability of the structure to distribute the load to the adjacent frames and on the length of the external loading. The same applies for the outermost instrumented frames when several frames are instrumented. Earlier studies have shown that the extent of the load in the horizontal direction can vary from one to several frame spacings (Hänninen et al., 2001; Suominen et al., 2017). Suominen et al. (2017) and Newmark (1938) discussed that the ratio between the frame and plating stiffness affects the ability of the structure to distribute loading to the adjacent frames.

Thus, the aim of this study is to determine the difference in the results when only one frame is instrumented in comparison to several frames when the length of the external load varies from a spacing of one frame to a spacing of several frames. In addition, the effect of the instrumentation on the statistical parameters of the measured ice load history, specifically the mean value, standard deviation and the coefficient of variation, will be analyzed. Chapter 2 describes the load transfer between frames. Chapters 3 and 4 study the sensitivity of the measurements on the extension of the instrumentation employing full-scale measurements on board polar supply and research vessel (PSRV) S.A. Agulhas II. The instrumented frames on board S.A. Agulhas II are considered to be instrumented separately and jointly. Finally, Chapter 4.5 presents a novel method to estimate the difference between an extensive and a narrow instrumentation.

2. Description of the load transfer between frames

In the ice breaking process, the bending failure of the ice sheet forms a cusp-like breaking pattern; see Fig. 1. Due to the pattern, the hull of the ship is partly in contact with ice and the location and length of the loading varies as the ship proceeds in the ice sheet. In the process, the ice induces a line-like pressure pattern at the contact locations for first-year ice (see e.g. Riska et al., 1990, Fig. 1) and high-pressure zones for thicker multi-year ice (see e.g. Jordaan, 2001; Taylor and Richard, 2014). The loading is transported and carried by the frames supporting the plate. The load causes a shear force on the frames; see Fig. 1. The loaded frame carries the majority of the loading. However, a part of the loading is transported by the plating to the adjacent frames and a part to the stiffer structure supporting the frames, such as stringers.

In the case of limited instrumentation, e.g. with one frame instrumented, the sensitivity of the measurement results on the length of the external loading is directly affected by the ability of the structure to transfer loading internally, as the response and conditions on the adjacent uninstrumented frames are not known. As discussed by e.g. Suominen et al. (2017) and Newmark (1938), the ratio of the frame and plating stiffness affects the amount of loading the loaded frame carries. Thus, this chapter presents the amount of load possibly transferred between the frames, which reflects the possible error related to the extension of the instrumentation in the measurements. Finite element (FE) and analytical methods are used for this.

2.1. Finite element analysis of the stiffened panels

The FE models implemented to study the load transfer are frame systems that consist of nine frames in total. Fig. 2 presents a sketch of the structure employed in the study cut in the line of symmetry, LS. The frame systems are simplifications of real structures. However, the systems are considered to represent the real side structure under ice loading with acceptable accuracy. The mesh size is 0.01 m. Pre- and post-processing were carried out with Femap and the linear-elastic solution with NX Nastran (version 10.3.1). In total 45 FE models were constructed, in which the frame spacing, s, the web height, h_W, the frame thickness, t_W, and the plate thickness, t_P, were varied; see Fig. 2 and Table 1. The length of the frame, L, is 1.5 m in each case. The selection of the cases was made starting from typical design spaces for ice-going vessels and then expanding from those. A 10-kN point load was applied at the middle of the model–see Fig. 2–for each structural configuration presented in Table 1. Clamped boundary conditions were applied for each structure at the outer edges of the plating and at the end of the

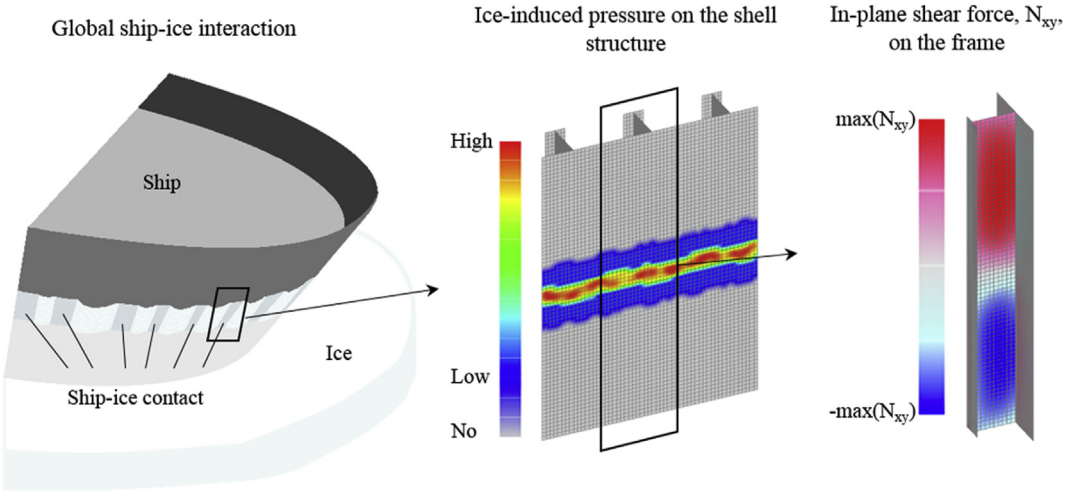

Fig. 1. Schematic illustration of the global ship-ice interaction, the ice-induced pressure on the shell structure and the resulting in-plane shear force, N_{xy}, on the frame.

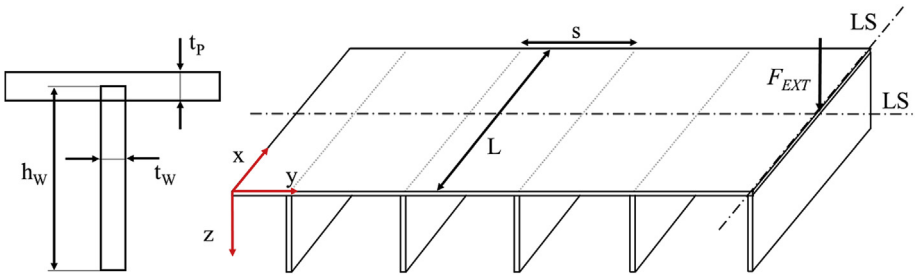

Fig. 2. The cross-section of a frame (on the left) and the frame system consisting of nine frames in total (on the right).

Table 1
The structural parameters in each case.

	Case #	s [m]	t_P [m]	h_W [m]	t_W [m]	Case #	s [m]	t_P [m]	h_W [m]	t_W [m]	Case #	s [m]	t_P [m]	h_W [m]	t_W [m]
Thin plate	1	0.3	0.01	0.2	0.01	19	0.4	0.01	0.2	0.01	37	0.6	0.01	0.2	0.01
	2	0.3	0.01	0.2	0.02	20	0.4	0.01	0.2	0.02	38	0.6	0.01	0.2	0.02
	3	0.3	0.01	0.2	0.03	21	0.4	0.01	0.2	0.03	39	0.6	0.01	0.2	0.03
Relatively thick plate	4	0.3	0.02	0.2	0.01	22	0.4	0.02	0.2	0.01	40	0.6	0.02	0.2	0.01
	5	0.3	0.02	0.2	0.02	23	0.4	0.02	0.2	0.02	41	0.6	0.02	0.2	0.02
	6	0.3	0.02	0.2	0.03	24	0.4	0.02	0.2	0.03	42	0.6	0.02	0.2	0.03
Thick plate	7	0.3	0.03	0.2	0.01	25	0.4	0.03	0.2	0.01	43	0.6	0.03	0.2	0.01
	8	0.3	0.03	0.2	0.02	26	0.4	0.03	0.2	0.02	44	0.6	0.03	0.2	0.02
	9	0.3	0.03	0.2	0.03	27	0.4	0.03	0.2	0.03	45	0.6	0.03	0.2	0.03
Thin plate	10	0.4	0.01	0.1	0.01	28	0.4	0.01	0.3	0.01					
	11	0.4	0.01	0.1	0.02	29	0.4	0.01	0.3	0.02					
	12	0.4	0.01	0.1	0.03	30	0.4	0.01	0.3	0.03					
Relatively thick plate	13	0.4	0.02	0.1	0.01	31	0.4	0.02	0.3	0.01					
	14	0.4	0.02	0.1	0.02	32	0.4	0.02	0.3	0.02					
	15	0.4	0.02	0.1	0.03	33	0.4	0.02	0.3	0.03					
Thick plate	16	0.4	0.03	0.1	0.01	34	0.4	0.03	0.3	0.01					
	17	0.4	0.03	0.1	0.02	35	0.4	0.03	0.3	0.02					
	18	0.4	0.03	0.1	0.03	36	0.4	0.03	0.3	0.03					

frames by fixing all the nodes for all the degrees of freedom $u = v = w = \theta_x = \theta_y = \theta_z = 0$. Furthermore, in order to study the effect of the boundary conditions that were employed, Cases 10 to 27 were additionally modelled with pinned boundary conditions $u = v = w = 0$, which were applied to the edges of the plating.

The shear force in the cross-section of the frame web is defined by integrating the in-plane shear force, N_{xy}, over the elements of the web in the height direction. The resulting shear force on the loaded frame and the adjacent frames, $Q_{x,FRAME}$, is presented in Fig. 3A and B, respectively. The shear force is presented from the end of the frame (the zero location) to the middle of the frame (0.75 m) where the 10-kN point load was applied to the loaded frame. Pinned boundary conditions were applied in Fig. 3. Case 21 represents a structure with a thin plate (10 mm) and a minor plate-frame bending stiffness ratio, D/I_F. Case 15 is chosen for a relatively thick plate thickness (20 mm) and a moderate bending stiffness ratio. Case 16 represents a thick plating (30 mm) where the stiffness ratio is great.

Fig. 3 shows that the shear force distribution on the adjacent frames adequately follows that of a line load. On the loaded frame, the shear force distribution along the frame is similar to that of a point load, Case 21, or combination of a point load and line load, Case 15 and 16. In the case of combined loading, the line load is a result of the supporting effect

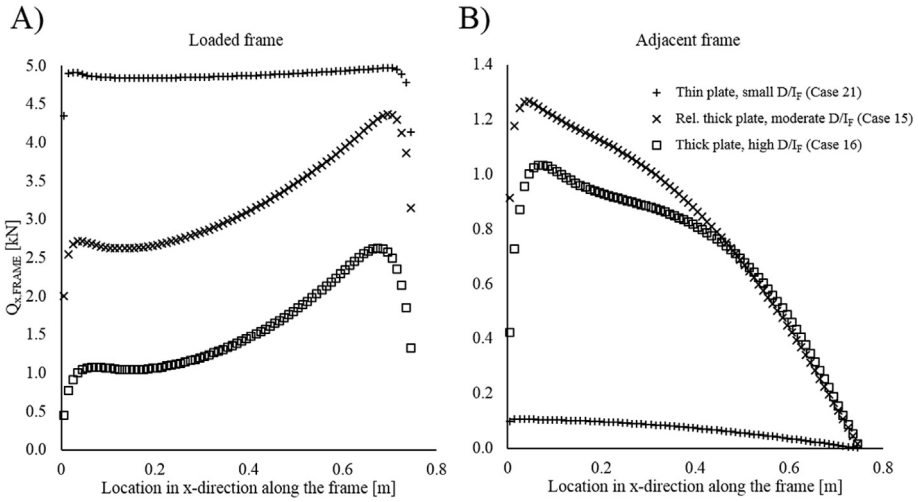

Fig. 3. The shear force in the cross-section of a frame determined with FEA as a function of the x-coordinate on the loaded frame (A) and on the adjacent frame (B).

of the adjacent frames. The amount contributed by the line load depends on the bending stiffness of the frame and plating, the frame spacing, and the length of the frame, see Chapter 2.2. The shear force at the ends of the beam for combined loading is *(F-qL)/2*. *qL* is considered to be the force transported from the loaded frame to the adjacent frames by the plating. As the loading on the frame is taken as the difference in the shear force between the ends of the frames, the load carried by the loaded frame is $Q_{FRAME} = F_{EXT}\text{-}qL$. Thus, the results in FEA are taken from this location.

2.2. The load distribution between frames

Suominen et al. (2017) developed a grillage model where the plating was considered as a longitudinal beam and the frames as transverse beams supporting the plating. They derived a solution for the load carried by the loaded frame, Q_{mid}, and the external force, F_{EXT}, for the simply supported case:

$$\frac{Q_{mid}}{F_{EXT}} = \frac{25k^2(20 - 126u + 125u^2) + 320k(10 - 81u + 145u^2) + 4096(1 - 9u + 19u^2)}{k_0} \tag{1}$$

Following the principles, the relation can be derived for the clamped boundary conditions as

$$\frac{Q_{mid}}{F_{EXT}} = \frac{k^2(68 - 470u + 625u^2) + 64k(22 - 187u + 350u^2) + 4096(1 - 10u + 23u^2)}{k_1} \tag{2}$$

The nominators are

$$\begin{aligned} k_0 &= 25k^3(4 - 6u + u^2) + 5k^2(356 - 2166u + 2129u^2) \\ &\quad +64k(82 - 645u + 1093u^2) + 4096(1 - 9u + 19u^2) \\ k_1 &= k^3(4 - 10u + 5u^2) + 3k^2(76 - 514u + 627u^2) \\ &\quad +192k(10 - 85u + 154u^2) + 4096(1 - 10u + 23u^2) \end{aligned} \tag{3}$$

The parameters k and u are related to the load distribution and rotation, respectively:

$$k = \frac{DL^4}{EI_F s^3} \text{ and } u = \frac{DL^2}{GCs} \tag{4}$$

where E = the Young's modulus, G = the shear modulus, I_F = the second moment of area of the frame, D = the bending stiffness of the plating, C = the rotational stiffness of the frame, L = the length of the frame, and s = the frame spacing.

As the factor k is related to the load transfer between frames, the load transfer is studied as a function of this factor. The relation between the shear force carried by the loaded frame and the external force was determined for the structures presented in Table 1 with Equations (1) and (2). The effective breadth of the plating employed in the bending stiffness calculation of the frame was defined with the design curve for a uniform line load as defined by Schade (1951, 1953). If the effective breadth is taken for the point load the term $DL^4/EI_F s^3$ is 7% smaller, on average, as a result of the decrease in the stiffness of the frame. As the results obtained with the grillage model followed a clear trend as a function of k, trend lines were fitted to the data. The type of curve shown in Equation (5), based on Equations (1) and (2), was fitted to the data:

$$f(k) = \frac{ak^2 + bk + c}{dk^3 + ek^2 + fk + c} \tag{5}$$

f(k) denotes the ratio Q_{mid}/F_{EXT} as a function of the factor k. The factors a, b, c, d, e, and f were evaluated with the MatLab2016a curve-fitting tool. The trend lines are plotted with the FEA results in Fig. 4.

Fig. 4 shows a very good correspondence between the FEA and grillage model results when the plate thickness is small. However, when the plate thickness increases to 30 mm, the results start to differ as the bending stiffness of the plate becomes non-negligible in comparison to that of the frame. In addition, Fig. 4 shows that the loading transported to the adjacent frames can be over 50% of the total loading for the structures presented in Table 1. The boundary conditions have a significant

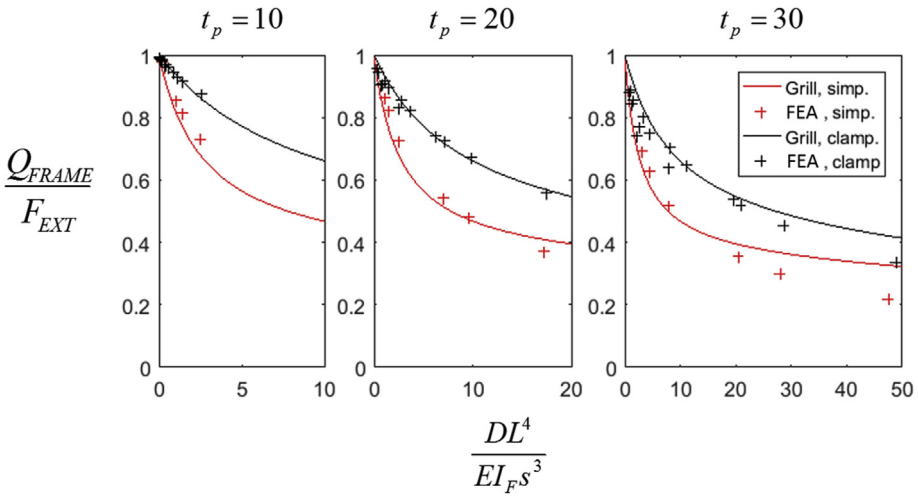

Fig. 4. The ratio of the loading carried by the loaded frame and external loading on the basis of the FEA and grillage model results.

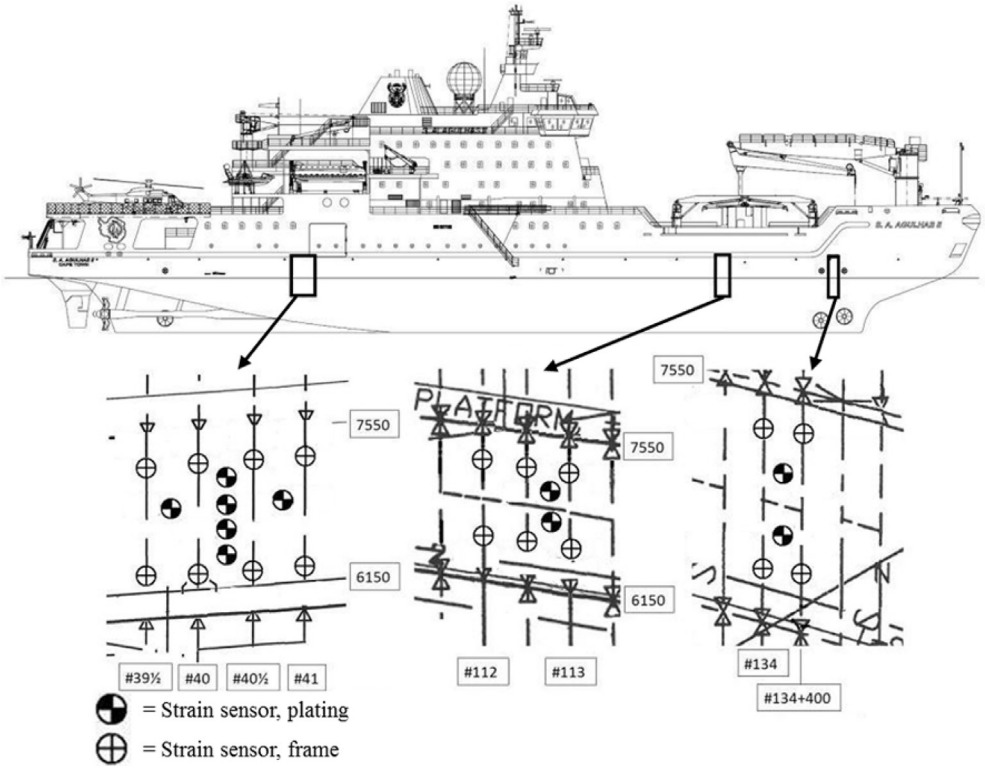

Fig. 5. Instrumentation of S.A. Agulhas II (Suominen and Kujala, 2015).

effect on the results as the fixed boundary conditions increase the stiffness of the frame in relation to the plate, which increases the amount of loading carried by the loaded frame.

3. Full-scale measurements on PSRV S.A. Agulhas II

PSRV S.A. Agulhas II was delivered from the Rauma Shipyard, Finland, to the Department of Environmental Affairs of South Africa in 2012. She was built to the polar ice class (PC) 5, while the hull was strengthened to the DNV ICE-10 class. During the construction, the bow, bow shoulder, and stern shoulder were instrumented for ice load measurements with fibre optic strain sensors with the capability to measure extreme ice-induced loads in the elastic region of the frame; see Fig. 5.

The study on this paper focuses on the stern shoulder, in which four adjacent frames were instrumented. The gauges on the frames #41, #40, and #39 were on the bow side of the frame; see Fig. 6. The gauges on the frame #40½ were mounted on the stern side. The gauges were located 0.3 m from the ends of the frame; see d_{low} and d_{up} in Fig. 7. The distances from the top of the web to the gauge, d_{web}, are given in Table 3. The structural parameters in the instrumented area are as follows: $L = 1.4$ m, $s = 0.4$ m, $h_w = 0.2$ m, $t_w = 0.019$ m, the hull plating thickness at the lower part of the frame, t_{p21}, $= 0.021$ m and at the upper part of the frame, t_{p20}, $= 0.020$ m, $E = 209$ GPa; and Poisson constant, ν, $= 0.3$ (Suominen et al., 2015). A more detailed description of the instrumentation is presented in Suominen et al. (2013, 2015, 2017).

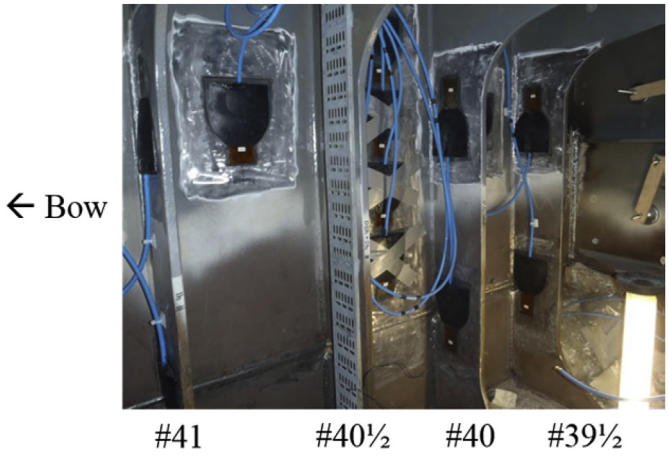

Fig. 6. Instrumentation at the stern shoulder before shielding.

The external load on the structure was determined from the measured shear strain difference with an influence coefficient matrix a and its inverse using the relations

$$\{F\} = [a]\{\Delta\gamma\} \text{ and } [c_{ij}] = \Delta\gamma_i(F_j) \quad (6)$$

where $\Delta\gamma_i$ $(i = 1 \ldots m)$ = the shear strain difference measured on the frame i, m = the number of instrumented frames, and F_j = the external force exerted on the frame j. The diagonal terms define the force-strain relation of the frame under loading and the off-diagonal terms determine the response of the adjacent frames. Thorough discussion of the determination of the ice loads by measuring shear strains is presented e.g. in Suominen et al. (2017).

The strain-force relation was determined by applying a 10-MPa pressure load to an area of 0.01 m*0.01 m. Table 2 and Equation (7) present the coefficients determined for each frame separately and the

Table 2
The structural response coefficients when frames are considered separately.

Frame	Coefficient
#41	320 × 103 kN/strain
#40½	317 × 103 kN/strain
#40	324 × 103 kN/strain
#39½	312 × 103 kN/strain

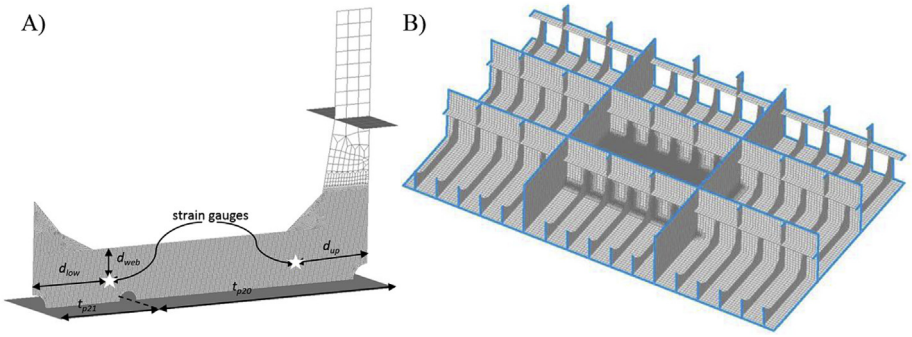

Fig. 7. The FE model applied in the study (Suominen et al., 2015, 2017).

influence coefficient matrix, respectively. The FE model was built using linear plate elements in Femap and the numerical calculations were conducted with NX Nastran (version 10.3.1). The finer mesh size was 0.005 m*0.005 m in the region of interest. The surrounding structure had a coarser mesh, with a mesh size 0.05 m*0.05 m. Rigid boundary conditions were applied to all the edges where the actual structure continued by constraining all degrees of freedom. The model was validated with the calibration pull; see Suominen et al. (2015, 2017). Table 3 presents the measured shear strains during the calibration pull with the modelled shear strains. As the system is scaled to measure over 1 MN loads, the measured shear strains at gauge locations are considered to be close to the modelled shear strains, see Table 3 for comparison.

$$a = \begin{bmatrix} 320.39 & 16.20 & -2.81 & 0.70 \\ 13.19 & 329.10 & -58.67 & 4.79 \\ 2.58 & -62.96 & 332.56 & 14.47 \\ -0.98 & 18.41 & -57.39 & 310.12 \end{bmatrix} * 10^3 kN/strain \quad (7)$$

4. The effect of external load length and instrumentation on the measured load in full-scale measurements

The full-scale data employed here was gathered on board PSRV S.A. Agulhas II during ice trials in the Baltic Sea in March 21–22, 2012. All the measurements and ice conditions during the trials are described by Suominen et al. (2013, 2014).

4.1. Calibration pull

Table 3 presents the measured strains and force for the calibration pull at the frame #40, and the strains modelled with FE model as described in Chapter 3. The sensors with even numbers are instrumented to the upper part of the frame. In addition, Table 3 presents the loads determined from the measured shear strains for the frames separately, see the coefficients in Table 2, and with the influence coefficient matrix, see Equation (7). A detailed description of the calibration pull is presented in Suominen et al. (2015, 2017). As shown in Table 3, the magnitude of the loading on the loaded frame, the frame #40, is estimated with good accuracy when the hull response is considered separately from the frame #40 and with the influence coefficient matrix accounting for all the instrumented frames. However, when the frames are considered separately, the frames #40½ and #39½ indicate external loading, although these frames were not loaded. When the influence coefficient matrix is applied, the loading is clearly on the frame #40 and only minor loading is present on the adjacent frames.

4.2. The effect on the measured time history of ice loading

Fig. 8 presents a narrow and wide load travelling over the instrumented area. The loading events start from the frame #41 and advance over the instrumented frames. Figs. 9 and 10 present the same events when the loading is determined for the frames separately and with the influence coefficient matrix approach. In Fig. 9 the loading is estimated to be one frame spacing wide, while the loading in Fig. 10 is approximately four frame spacings wide. The small structural pictures inside the figures illustrate the estimated location of the loading at different times, t. The load distribution, width, and locations in these pictures are added here for illustrative purposes. Thus, they should not be considered exact.

When a narrow loading is approaching and acting on the frame #41, the loading is the same when the frames are considered separately and when the influence coefficient matrix is applied; see Fig. 9. A similar trend can be seen for the frame #39½ when the load is leaving the instrumented area. The time histories for the frames #40½ and #40 show small differences in the results. A similar behaviour is observed for a wide loading case; see Fig. 10. At first, the separate consideration of frames and an influence coefficient matrix give similar results for the frame #41, but the results begin to differ when the loading reaches the frame #40½. For the frames #40½ and #40 the separate consideration and the influence coefficient matrix give slightly different results and for the frame #39½ the results differ as long as the loading is no longer affecting the frame #40. This highlights the ability of the influence coefficient matrix to account for the conditions at adjacent frames.

The observed similarities and differences demonstrate how the influence coefficient matrix takes into account the measured strains on all the instrumented frames when the loading on a frame is determined. When the loading affects outside the instrumented area or partly the outermost frames, namely the frames #41 and #39½, the only frames

Table 3
Calibration pull on frame #40.

Frame		#41		#40½		#40		#39½	
Sensor	Name	SS16	SS17	SS18	SS19	SS20	SS21	SS22	SS23
	Distance to the tip of the web [m]	0.120	0.125	0.124	0.117	0.125	0.120	0.120	0.130
Calibration pull	Measured strain [μstrain]	0.22	0.27	6.11	−4.56	23.29	−23.67	5.10	−3.94
	Measured force [kN]					15.55			
FEA	Modelled strain [μstrain]	0.00	0.03	3.96	−4.35	23.10	−24.82	3.95	−4.31
Determined loading	Separate frames, Force [kN]	−0.02		3.38		15.22		2.82	
	Influence coefficient matrix, Force [kN]	0.03		0.80		15.08		0.31	

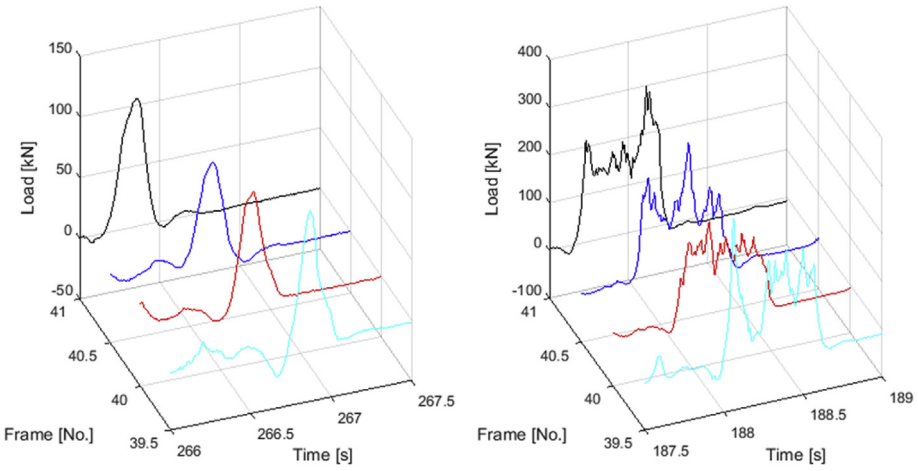

Fig. 8. A narrow and wide load travelling over the instrumented area on the left and right, respectively. The loading determined with the influence coefficient matrix approach.

responding to the external loads are these frames. As the frames #41 and #39½ are the only ones responding, the determined loading is approximately the same when the frames are considered separately and with the influence coefficient matrix. When the loading is acting between the outermost frames in the instrumented area, the shear strains are recorded on more than one instrumented frame, which affects the results obtained with the influence coefficient matrix. The difference is partly due to the load distribution between the frames and partly due to the variation in the location of the loading. When the loading travels from one frame to another, e.g. from the frame #40½ to #40, and acts in the middle, the loading has a partial effect on both frames. In these situations, the influence coefficient matrix takes into account the situation at adjacent instrumented frames, while the separate consideration of the frames neglects this.

4.3. *The effect on the peak load magnitude*

The load length has been defined in two steps (see Suominen et al., 2017). At first, separate loading events were identified from the frames #40½ and #40 by applying Rayleigh separation; see Suominen and Kujala (2014). The separation compares the minimum loading between the two consecutive load maxima in the measured time history. If the minimum is smaller than the smaller maximum multiplied by the separator value, the two maxima are considered to originate from separate

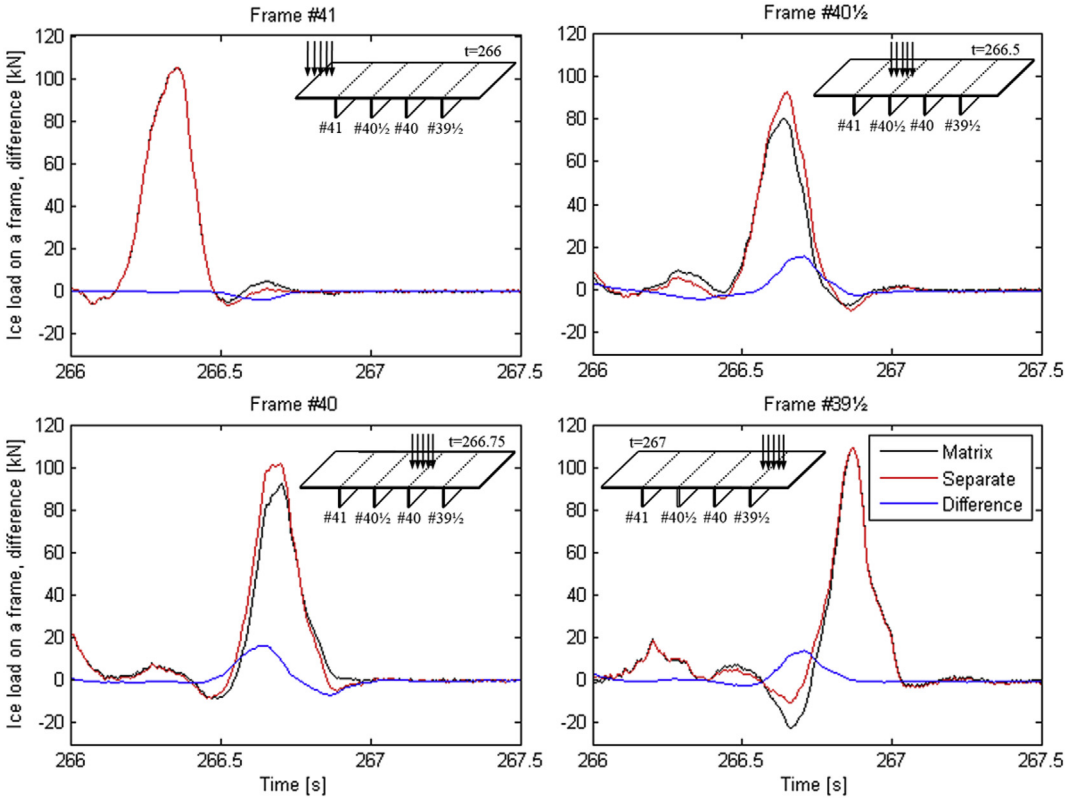

Fig. 9. The load time history for the frames under a narrow external loading when the frames are accounted for separately and jointly with the influence coefficient matrix and the labed as Separate and Matrix, respectively. Difference denotes the difference in the results.

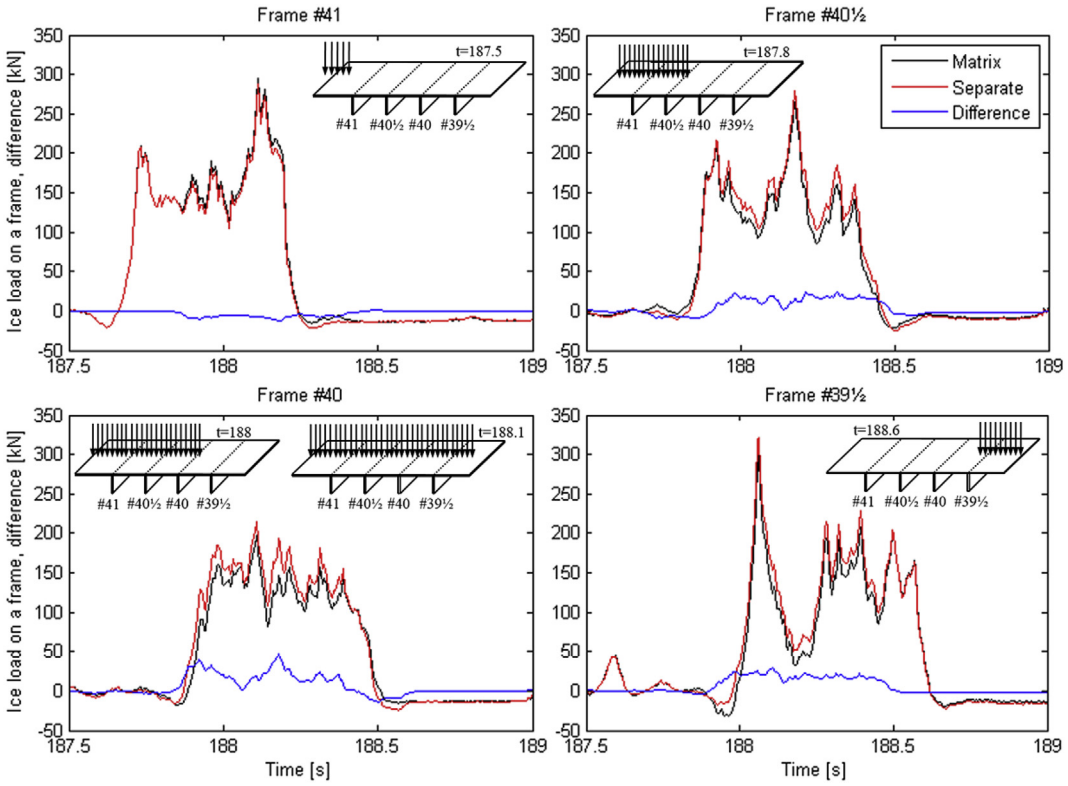

Fig. 10. The load time history for the frames under a wide external loading when the frames are accounted for separately and jointly with the influence coefficient matrix labed as Separate and Matrix, respectively. Difference denotes the difference in the results.

loading events. A threshold can be applied to disregard the noise in the measurements. In the second phase, the loading conditions on all the frames, i.e. #41-#39½, were observed at the time instant the maximum was recorded on the frame #40½ or #40. The load length was taken as the number of adjacent frames on which the loading exceeded the applied threshold.

This study employs the load events identified by Suominen et al. (2017) for different load lengths with a threshold of 10 kN and a separator value of ½. At first, the measured shear strains from the loading events identified by Suominen et al. (2017) were gathered. Then the loadings on the frames #40½ and #40 were determined from the strains when the frames were considered separately and jointly with the influence coefficient matrix. When the frames were considered separately, the strains were observed only on these frames and the conversion to loads was performed by applying the coefficients presented in Table 2. When the frames were considered jointly, the strains on all the frames were

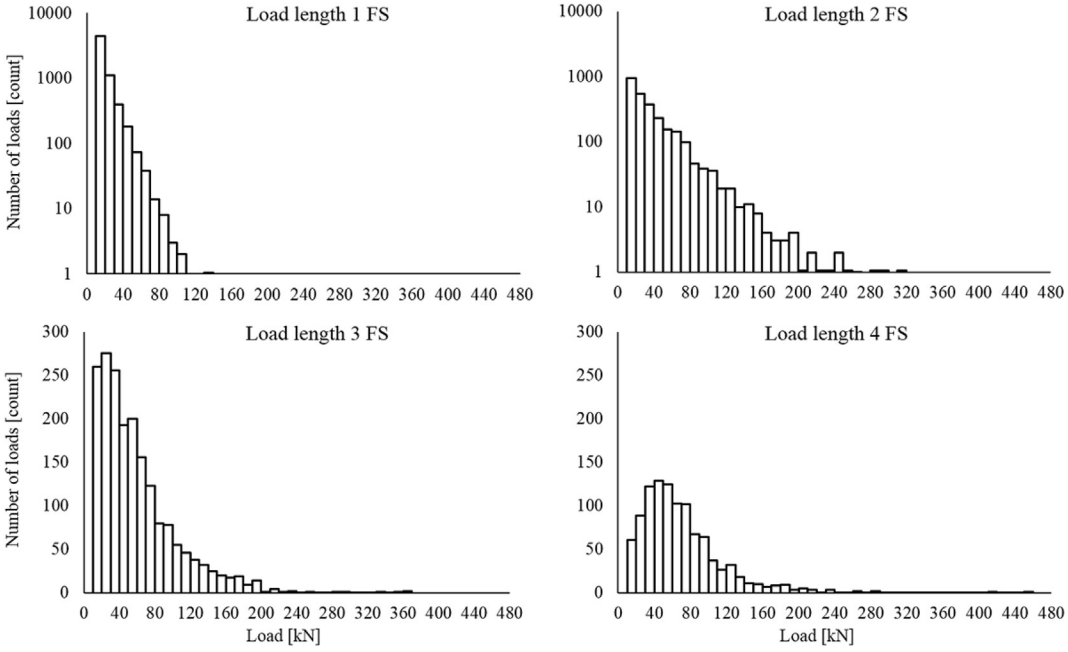

Fig. 11. The number of load events on the frames #40½ and #40 identified by Suominen et al. (2017) for different load lengths. Note the logarithmic scale on the y-axis of the upper plots.

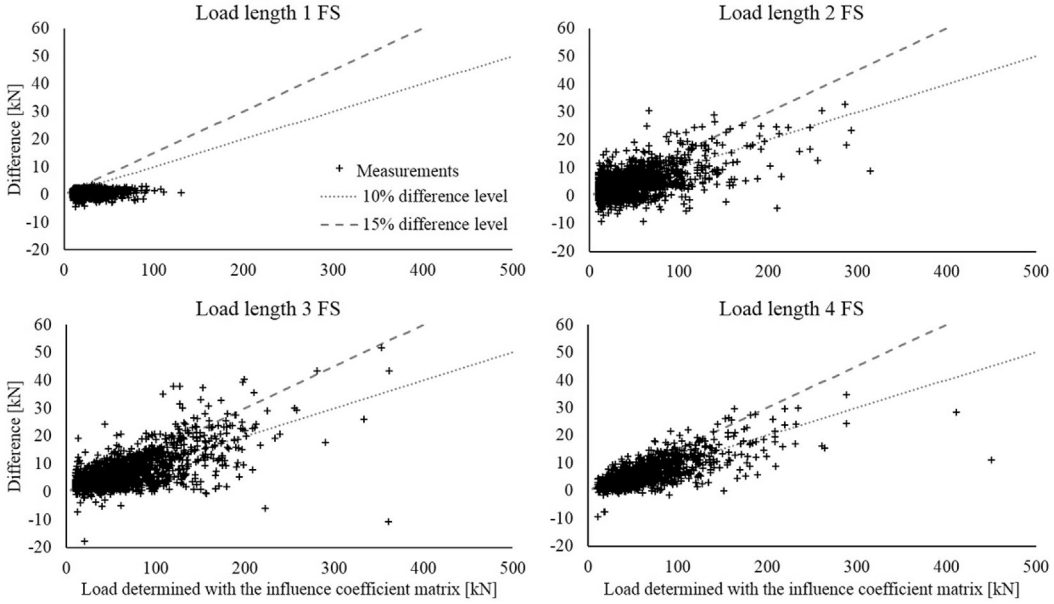

Fig. 12. The difference in the determined load magnitude as a function of the load determined with the influence coefficient matrix for different load lengths.

observed and the loading on the frames #40½ and #40 was determined with Equation (7), i.e. with the influence coefficient matrix. Fig. 11 presents the histograms of load events for different load lengths determined with the influence coefficient matrix. Note that for the shorter loads (1 FS and 2 FS) the load distribution is exponential-like, but for longer loads (3 FS and 4 FS) the distribution is lognormal-like. After the load on the frame on each event was determined with the influence coefficient matrix and frames separately, the differences in the results were calculated. Fig. 12 presents the differences for different load lengths. Positive values indicate that the magnitude is higher when the frames are considered separately.

As can be noted, the difference is insignificant for loading events that are one frame spacing wide, but the difference increases for the wider and higher-magnitude loading cases. The relative difference is greater for smaller loading magnitudes, but is also significant for higher loading magnitudes. The magnitude determined for separate frames can be approximately 15% higher than the magnitude obtained with the matrix for loading events greater than 300 kN. The differences in the results presented in Fig. 12 were organized into ranges based on the histograms presented in Fig. 11 and the mean value and standard deviation of the differences in each range were calculated. The ranges with fewer than three samples were disregarded from the calculations. The results of these calculations show a similar trend to that in Fig. 12; see Fig. 13. The average difference for loads one frame spacing wide and for small loads with a wider loading is close to zero and the scatter is insignificant. However, the mean difference and standard deviation increase as a function of the load magnitude; see Figs. 11 and 13.

4.4. The effect on the statistical parameters of the 5-min measured period

The strains were recorded in 5-min continuous time histories with 200 Hz. The continuous strain time histories were converted into ice-

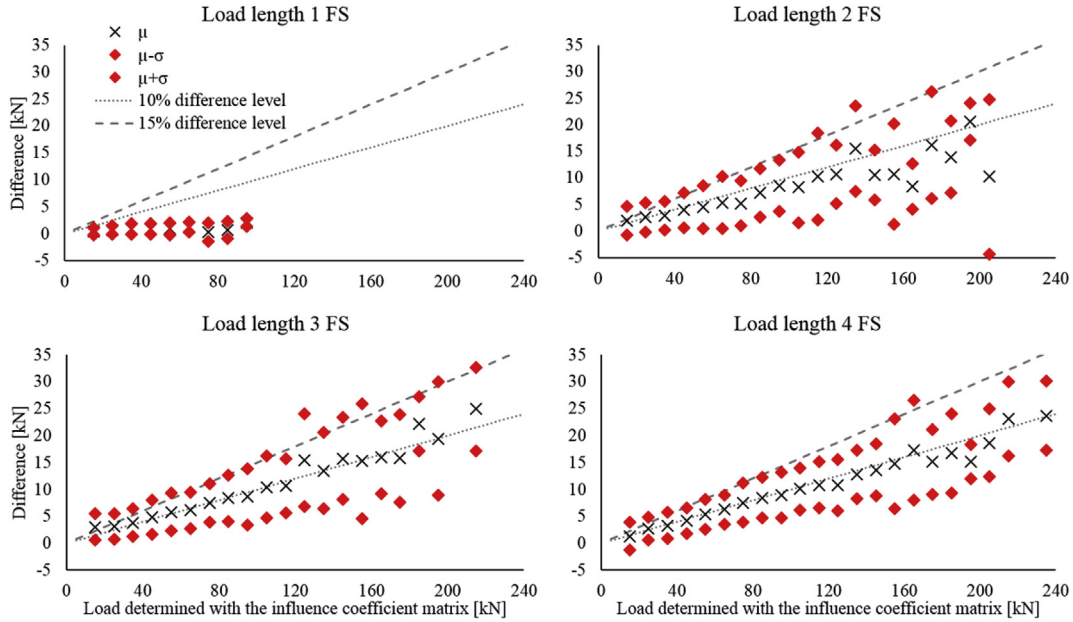

Fig. 13. The mean difference, μ, of the loads classified into 10-kN bins on the basis of the measured load with the matrix. σ denotes the standard deviation of the difference in the load bin.

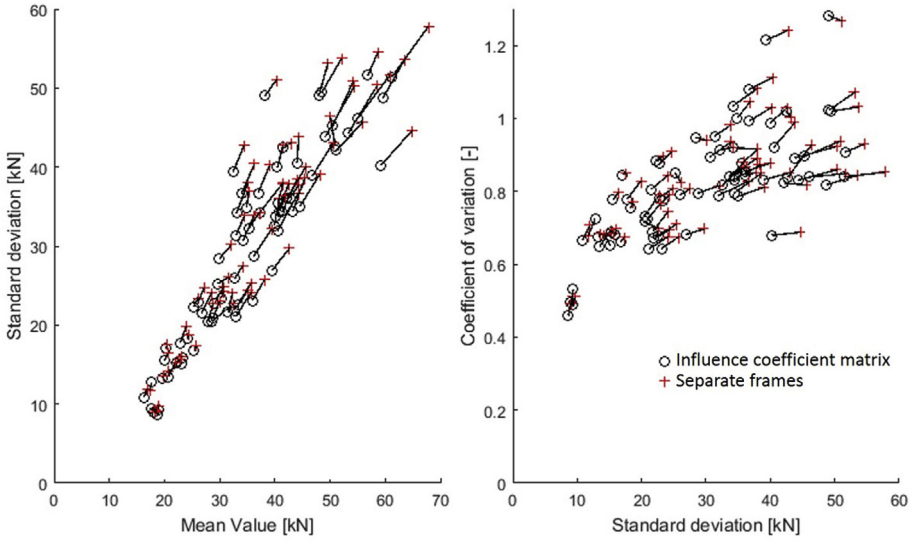

Fig. 14. The standard deviation as a function of the mean value, on the left, and the coefficient of variation as a function of the standard deviation, on the right, from the same 5-min period. The lines indicate which solutions are from the same 5-min period.

induced load time histories as described in Chapter 3, with the frames being considered both separately and with the influence coefficient matrix. Then the ice-induced loads were identified from the time history with Rayleigh separation. The applied factor and threshold in Rayleigh separation were ½ and 10 kN, respectively. After the load events were identified, the mean values, standard deviation, and coefficient of variation were calculated for each period. As the calculation of the statistical parameters is more relevant for cases with a number of samples, the parameters were calculated only for the periods for which more than 50 load events were identified with both methods (there is no theoretical basis for setting the number at 50). It was observed that with a lower limit of 50 peaks the number of remaining periods was still reasonable. The statistical parameters are presented in Fig. 14. Fig. 15 presents the differences in the statistical parameters that correspond to the length of the lines connecting the parameters in Fig. 14.

Kujala et al. (2009) and Suominen and Kujala (2014) observed that the mean values of measured ice loads follow a linear-like trend as a function of standard deviation. This can be explained by assuming that all the periods share the same initial mean value and each period has its own unique peak (Suominen and Kujala, 2014). In the case of a short-term ice-induced load, the distribution of the load amplitude is exponential. Thus, the initial mean value approaches the threshold of the measurements and the initial standard deviation approaches zero. The unique value corresponds to the maximum value of the period. The number of peaks for the period defines the slope of the linear-like trend. The mean value and standard deviation of the final set of samples, $\bar{x}_L$ and σ_L, can be presented as a function of the initial mean value and standard deviation, $\bar{x}_A$ and σ_A, the number of samples in the initial set, n, and the added value, i.e. maximum x_{n+1}, as follows:

$$\bar{x}_L = \frac{1}{n_L}\sum_{i=1}^{n_L} x_i = \bar{x}_A + \frac{x_{n+1} - \bar{x}_A}{n+1} \tag{9}$$

$$\sigma_L = \sqrt{\frac{\sum_{i=1}^{n_L}(x_i - \bar{x}_L)^2}{n_L - 1}} = \sqrt{\sigma_A^2 - \frac{\sigma_A^2}{n} + \frac{(x_{n+1} - \bar{x}_A)^2}{n+1}} \tag{10}$$

For further observations and discussion, see Suominen and Kujala (2014).

Fig. 14 shows the same trend as that observed by Suominen and Kujala (2014). The differences are minor for smaller values of statistical parameters, but increase for higher values, being up to 10% higher for separate frames. Generally, when the loads are defined separately for separate frames, the mean values and standard deviations are higher; see

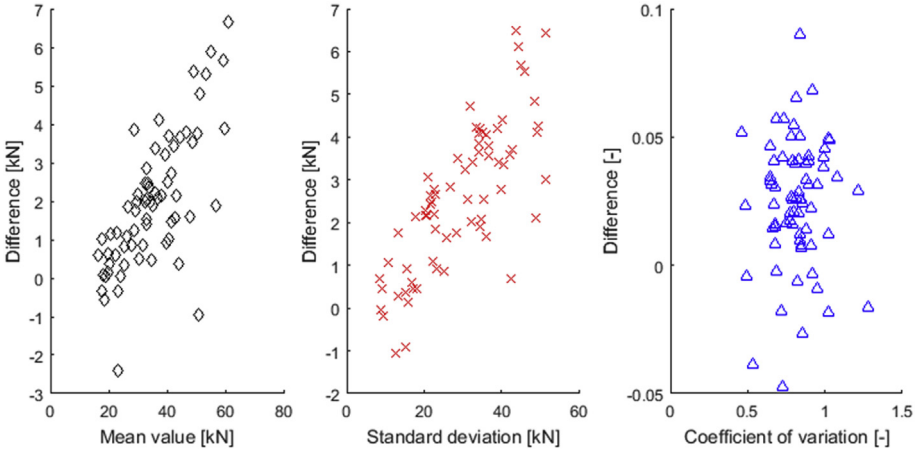

Fig. 15. The difference in the mean value, standard deviation, and coefficient of variation determined with the influence coefficient matrix and frames separately as a function of the values determined with the influence coefficient matrix.

Figs. 14 and 15. The difference in the coefficient of variation is not as significant as both the mean value and standard deviation are higher for separate frame consideration. However, on average, the coefficient of variation increases slightly for separate frames; see Fig. 15. As noted above, the difference between the influence coefficient matrix and separate frames is insignificant for narrow loads and increases for longer load lengths. Suominen et al. (2017) showed that the highest loads on a single frame occur when the external loading is wide. Thus, the greater difference in the higher values of the statistical parameters between the separate frames and matrix results is expected to be due to the maximum load occurring with longer load lengths. Furthermore, the difference is insignificant for smaller statistical parameter values, as the load lengths are generally narrow.

4.5. Estimation of the possible error in the full-scale measurements

The possible error in the measurements can be estimated with the method presented in Chapter 2. Fig. 4 show the ratio of the loading the loaded frame carries. The load-carrying ratio is presented as a function of the factor k. The factor k depends on the ratio between the bending stiffness of the plate and frame and the ratio between the frame spacing and frame length. Fig. 4 shows that the load-carrying ratio decreases rapidly at small values of k. The possible error in the measurements related to the extension of the instrumentation and the length of the external loading depends on the ability of the structure to transfer loading internally. Thus, the possible error increases rapidly at smaller values of k. This suggests that when structures with higher values of k are instrumented, three adjacent frames should be the minimum extension of the instrumentation. In this case, the middle frame would give results that are more accurate.

Chapter 3 presented the structural parameters needed to calculate k for the aft shoulder of S.A. Agulhas II. k obtains values of 1.05 and 1.08 for the simply supported and clamped cases, respectively. Implementing these into Equation (5), the loading carried by the loaded frame is 81% for the simply supported case and 93% for the clamped cases. As the reality is somewhere between these two, we can conclude that for the aft shoulder structure of S.A. Agulhas II, the transportation of the load to the adjacent frames is not tremendous, but notable. Following the same procedure, the possible difference is calculated for different structures. Table 4 presents the structural parameters needed for the evaluation for motor ship (MS) Kemira, motor tanker (MT) Uikku, and PSRV S.A. Agulhas II. Fig. 16 presents the possible error for the structures with the curves for the grillage model.

In the case of PSRV S.A. Agulhas II, the amount of loading transferred to the adjacent frames is higher for the bow in comparison to aft, as the hull plating is significantly thicker, although the frame is significantly stiffer. However, the comparison in Fig. 4 shows that the results differ between the FEA and the grillage model at these plate thicknesses. The instrumentation on board MS Kemira and MT Uikku consisted of frames in three areas of the hull, but only one frame in these areas was instrumented (Kujala, 1989; Kotisalo and Kujala, 1999). MT Uikku's mid-section is not considered here as it was longitudinally framed. Fig. 16 shows that the internal load distribution is significant for MS Kemira and MT Uikku. As the reality is something between the clamped and simply supported boundary conditions, the load distribution between the frames is taken as an average of the two boundary conditions. Focusing on the mid-section of MS Kemira, the load carried by the loaded frame is 70% of the external loading.

Table 4
Structural parameters for MS Kemira, PSRV S.A. Agulhas II, and MT Uikku. Information collected from Kujala (Kemira: 1994, Table 3; 1989, Fig. 2; Uikku: 1991, ships 48–50 in Fig. 33), and S.A. Agulhas II from drawings.

Ship and area	Frame spacing [m]	Frame span [m]	Frame profile [mm]	Plate thickness [mm]
MS Kemira, bow	0.37	2.68	L-300 × 11.5/ 100 × 16	21
MS Kemira, midship	0.35	2.5	L-250 × 10/90 × 10	16
MS Kemira, aft	0.356	2.51	L-200 × 12/ 100 × 12	16
PSRV S.A. Agulhas II, bow	0.4	2.4	T-400 × 17/ 100 × 12	28
PSRV S.A. Agulhas II, aft	0.4	1.4	I-200 × 19	21/20
MT Uikku, bow	0.35	2.5	HP 320 × 13	24
MT Uikku, aft	0.35	2.5	HP 240 × 10	15

Considering the instrumentation of one frame, we apply two calibration cases. In the first case, the shear strain-force relation is determined from a concentrated loading affecting only one frame; see Fig. 17A. In the second case, the response is determined from a wide uniform load that is represented in Fig. 17B as concentrated loads affecting several adjacent frames. In the first case, the shear strain on the observed frame that corresponds to a load of 1 F equals 0.7 F. In the second case, the shear strain on the observed middle frame corresponding to 1 F is 1 F. If we now use the calibration for a concentrated loading (the first case), the concentrated loadings are measured correctly. However, if the external loading is wide, the loading is overestimated. If the external loading equalled the case presented in Fig. 17B, the calibration presented in Fig. 17A would indicate the external load to be 100%/70% *F ≈ 1.43 F. Conversely, if the calibration is from a wide loading case, the wide external loads are determined correctly, but the narrow ones are underestimated. If the external loading were as presented in Fig. 17A and the calibration from the case presented in Fig. 17B, the external loading on the middle frame would be 70%/100%*F = 0.7 F. The strain-force relation coefficients applied in the measurements of MS Kemira were determined by employing a loading two frame spacings wide, 0.7 m, that was 0.3 m in height (Kujala, 1989). Kujala (1989) reported that if the loads are shorter than two frame spacings, the system can give loads that are up to 30% too small. Although the case presented in Fig. 17B does not correspond exactly to the loading that was applied, the results are very close.

5. Conclusions

The study aimed to determine the difference in the measured ice loads when only one frame is instrumented in comparison to several frames. In the study, the length of the external load varied from a spacing of one frame to a spacing of several frames. The study showed that when the external loading affects only one frame, the effect of the extension of the instrumentation is insignificant. However, an increase in the load length increases the difference and can be approximately 15% higher for one frame instrumentation as the loading conditions on the adjacent frames are not accounted for. Furthermore, the 5-min measured mean value and standard deviation can be up to 10% higher for the one frame instrumentation. The possible error of the full-scale data is important for both evaluation of the measured maxima as well as for the statistical characteristics of the measured load values.

The observed difference in measured ice-loads is due to the ability of the structure to transport loading from the adjacent frames to the observed frames. The portion of the external load transported to the adjacent frames increases as a function of the ratio between the stiffness of the plate and frame, and the ratio between the frame length and spacing. Thus, the possible error increases as a function of these ratios. As a follow-up, the study presented a novel method to obtain a rough estimate on the possible error in the measurements. The method was applied in earlier full-scale measurements. As the results show, the possible error in the full-scale measurements on board MS Kemira (Kujala, 1989) and MT Uikku (Kotisalo and Kujala, 1999) is significant. The method can be also applied in the decision making when the extent of the instrumentation for full-scale measurements is being determined.

To the best of the authors' knowledge, this is the first study to

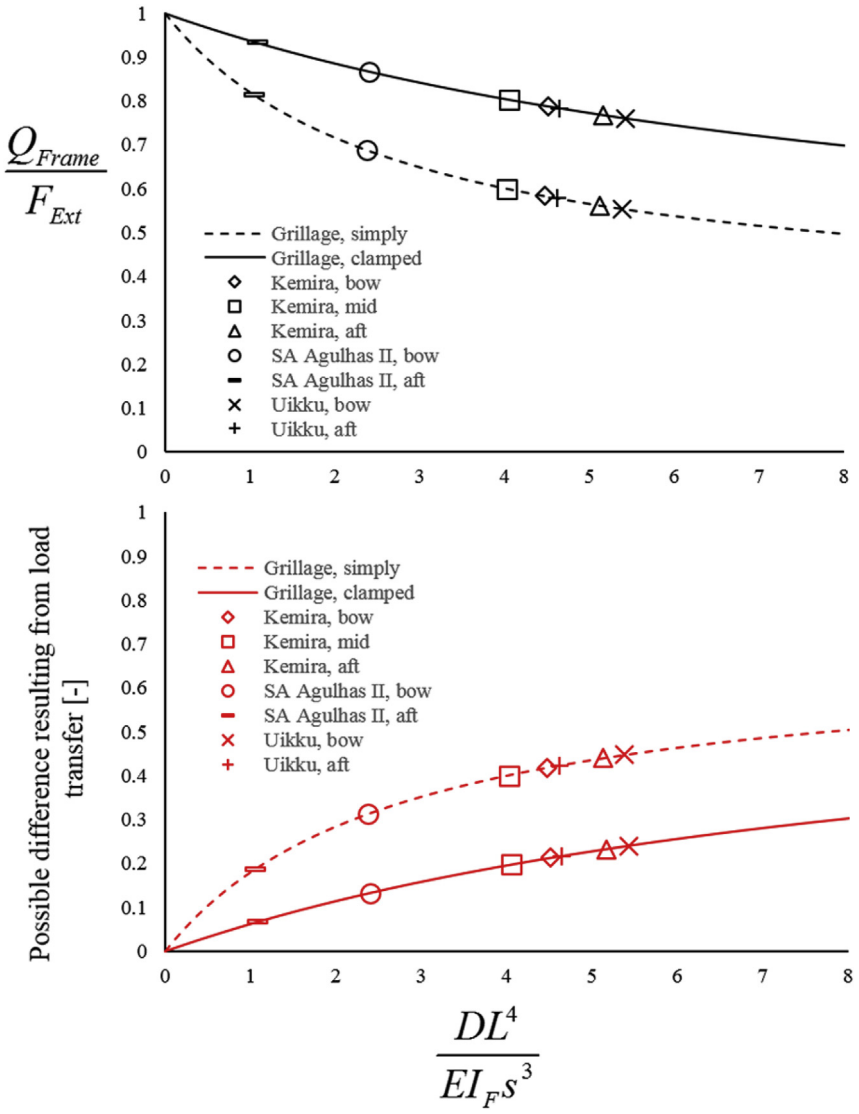

Fig. 16. At the top, the amount of loading carried by the loaded frame. At the bottom, the possible error resulting from load transfer between frames when one frame is instrumented.

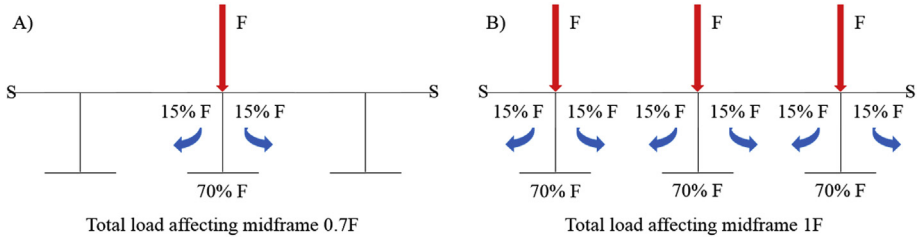

Fig. 17. Internal load distribution between frames when the loaded frame carries 70% of the external loading, for a narrow loading case (A) and a wide loading case (B).

highlight the importance of this topic and investigate it extensively through full-scale measurements. However, it should become a standard procedure when full-scale measurements are conducted and reported. However, the method applied to estimate the possible error is not accurate when the hull plating is thick (over 0.03 m). The improvement of the method is left for future studies. The study also focused only on variation in the horizontal direction. The variation in the location and extent in the vertical direction that could result in contact problems is left for future studies. The assumption about the loading condition applied for the strain-force determination also has a significant impact on the loading that is determined. A concentrated loading gives a less conservative estimation of the loading. The effect of the assumed loading condition on the loading that is determined is left for future studies.

Acknowledgements

The work was funded by the Finnish Funding Agency for Technology and Innovation (grant decision 40508/11), Academy of Finland (grant 264354), and the Lloyd's Register Foundation (the grant for Centre of Excellence for Arctic Shipping and Operations). The Lloyd's Register Foundation supports the advancement of engineering-related education, and funds research and development that enhances the safety of life at

sea, on land, and in the air. Their financial support is gratefully acknowledged. In addition, the University of Oulu, University of Stellenbosch, Aker Arctic, Rolls-Royce, STX Finland, Wärtsilä, and the Department of Environmental Affairs (South Africa), as partners of the Tekes project NB1369 Full-scale ice trial, and the Finnish Meteorological Institute, as a partner of the Academy of Finland project ANTLOAD, are gratefully acknowledged.

References

Ehlers, S., Cheng, F., Kuehnlein, W., Jordaan, I., Kujala, P., Luo, Y., Riska, K., Sirkar, J., Oh, Y., Terai, K., Valkonen, J., Ralph, F., 2015. 19th International Ship and Offshore Structures Congress Committee V.6 Arctic Technology. Cascais, Portugal, September 7-10, 2015, pp. 770–816.

Gagnon, R., 2008. Analysis of data from bergy bit impacts using a novel hull-mounted external Impact Panel. Cold Reg. Sci. Technol. 2008 (52), 50–66.

Hänninen, S., Lensu, M., Riska, K., 2001. Analysis of the Ice Load Measurements during USCGC Healy Ice Trials, Spring 2000, 2001. Helsinki University of Technology, Ship Laboratory, Report M-265, Espoo, Finland, p. 2001.

Jordaan, I., 2001. Mechanics of ice-structure interaction. Eng. Fract. Mech. 2001 (68), 1923–1960.

Kim, H., Quinton, B., 2016. Evaluation of moving ice loads on an elastic plate. Mar. Struct. 50, 127–142 (2016).

Kotisalo, K., Kujala, P., 1999. Ice Load Measurements Onboard MT Uikku, Measurements Results from the ARCDEV-voyage to Ob-estuary, April-may 1998. Report from WP8 of ARCDEV project supported by the EC Transport programme, Espoo, Finland.

Kujala, P., Vuorio, J., 1986. Results and Statistical Analysis of Ice Load Measurements on Board Icebreaker Sisu in Winters 1979 to 1985. Winter Navigation Research Board, Research Report No 43. Helsinki, Finland; 1986.

Kujala, P., 1989. Results of Long-term Ice Load Measurements on Board Chemical Tanker Kemira in the Baltic Sea during the Winters 1985 to 1988. Winter Navigation Research Board, Research report No 47. Helsinki, Finland; 1989.

Kujala, P., 1991. Damage Statistics of Ice-strengthened Ships in the Baltic Sea 1984-1987. Winter Navigation Research Board, Research report No 50. Helsinki, Finland; 1991.

Kujala, P., 1994. On the statistics of ice loads on ship hull in the Baltic, Acta Polytechnica Scandinavica. Doctoral dissertation. In: Mechanical Engineering Series No. 116. Helsinki; 1994.

Kujala, P., Suominen, M., Riska, K., June 9-12, 2009. Statistics of Ice Loads Measured on MT Uikku in the Baltic. In: Proceedings of the 20th International Conference on Port and Ocean Engineering under Arctic Conditions (POAC), Luleå, Sweden.

Newmark, N., 1938. A Distribution Procedure for the Analysis of Slabs Continuous over Flexible Beams. University of Illinois Bulletin No. 304, Urbana, Illinois, USA.

Ralph, F., Ritch, R., Daley, C., Browne, R., 2003. Use of finite element methods to determine iceberg impact pressure based on internal strain gauge measurements. In: Proceedings of the 17th International Conference on Port and Ocean Engineering under Arctic Conditions (POAC). Trondheim, Norway, June 16-19, 2003.

Riska, K., Kujala, P., Vuorio, J., 1983. Ice load and pressure measurements on board I.B. Sisu. In: Proceedings of the 7th International Conference on Port and Ocean Engineering under Arctic Conditions (POAC), Espoo, Finland; 1983;2, pp. 1055–1069.

Riska, K., Rantala, H., Joensuu, A., 1990. Full Scale Observations on Ship-ice Contact Results from Tests Series Onboard IB Sampo, Winter 1989. Helsinki University of Technology, Laboratory of Naval Architecture and Marine Engineering. Report M-97, Espoo, Finland; 1990.

Ritch, R., Frederking, R., Johnston, M., Browne, R., Ralph, F., 2008. Local ice pressures measured on a strain gauge panel during the CCGS Terry Fox bergy bit impact study. Cold Reg. Sci. Technol. 2008 (52), 29–49.

Sanderson, T., 1988. Ice Mechanics: Risk to Offshore Structures. Graham & Trotman, London, UK, 1988.

Schade, H., 1951. The effective breadth of stiffened plating under bending loads. Trans. SNAME 1951 (59), 403–420.

Schade, H., 1953. The effective breadth concept in ship structure design. Trans. SNAME 1953 (61), 410–430.

Ship Structure Committee, 1990. Ice Loads and Ship Response to Ice, Summer 1982/ Winter 1983 Test Program. Ship Structure Committee report SSC-329; 1990.

St John, J., Sheinberg, R., Ritch, R., Minnick, P., 1994. Ice impact load measurement abroad the Oden during the international Arctic ocean expedition 1991. In: Proceedings of 5th International Conference on Ships and Marine Structures in Cold Regions (ICETECH). SNAME, Calgary, Alberta, Canada. March 16-18, 1994.

Su, B., Riska, K., Moan, T., 2011. Numerical simulation of local ice loads in uniform and randomly varying ice conditions. Cold Reg. Sci. Technol. 2011 (65), 145–159.

Suominen, M., Karhunen, J., Bekker, A., Kujala, P., Elo, M., von Bock un, Polach, R., Endlund, H., Saarinen, S., 2013. Full-scale measurements on board PSRV S.A. Agulhas II in the baltic sea. In: Proceedings of the 22nd International Conference on Port and Ocean Engineering under Arctic Conditions (POAC). Espoo, Finland, June 9-13, 2013.

Suominen, M., Kujala, P., 2014. Variation in short-term ice-induced load amplitudes on a ship's hull and related probability distributions. Cold Reg. Sci. Technol. 2014 (106-107), 131–140.

Suominen, M., Kulovesi, J., Lensu, M., Lehtiranta, J., Kujala, P., 2014. A comparison of shipborne methods for ice thickness determination. In: 22nd IAHR Int. Symposium on Ice. Singapore, August 11-15, 2014.

Suominen, M., Romanoff, J., Remes, H., Kujala, P., 2015. The determination of ice-induced loads on the ship hull from shear strain measurements. In: Proceedings of the 5th International Conference on Marine Structures (MARSTRUCT). Southampton, UK, March 25-27, 2015.

Suominen, M., Kujala, P., 2015. The measured line load as a function of the load length in the Antarctic Waters. In: Proceedings of the 23rd International Conference on Port and Ocean Engineering under Arctic Conditions (POAC). Trondheim, Norway, June 14-18, 2015.

Suominen, M., Kujala, P., Romanoff, J., Remes, H., 2017. Influence of load length on short-term ice load statistics in full-scale. Mar. Struct. 2017 (52), 153–172.

Taylor, R., Jordaan, I., Li, C., Sudom, D., 2010. Local design pressure for structures in ice: analysis of full-scale data. J. Offshore Mech. Arct. Eng. 132. Aug 2010.

Taylor, R., Richard, M., 2014. Development of a probabilistic ice load model based on empirical descriptions of high pressure zone attributes. In: 33rd Int. Conf. On Ocean, Offshore and Arctic Engineering. San Francisco, USA; 2014.